# The Effect of Riboflavin and Blue Laser Irradiation on B16-F10 Melanoma Cell Death

**Aigul K. Gilmutdinova*, Elena V. Iurova, Evgeniya V. Pogodina, Anna V. Khokhlova, Dmitry E. Sugak, and Yury V. Saenko**

Federal State Budgetary Educational Institution of Higher Education "Ulyanovsk State University", 42 L. Tolstoy str., Ulyanovsk 432017, Russian Federation

*e-mail: gilmutdinovaajjgul@gmail.com

**Abstract.** Riboflavin, a natural photosensitizer, is of significant interest for the development of low-toxicity photodynamic therapy (PDT) protocols. This study is focused on the evaluation of the cytotoxic effect and ionic imbalances in B16-F10 melanoma cells induced by riboflavin when irradiating with blue laser light (450 nm wavelength). The dynamics of cell death and changes in intracellular sodium, potassium, and calcium ion concentrations were analyzed with the use of fluorescence microscopy. At a riboflavin concentration of 50 μM under laser irradiation, the signal corresponding to early apoptotic features in B16-F10 cells increased by 2.2 times compared to the control group. The maximum increase associated with late apoptosis and necrosis was observed 6 h after exposure and exceeded the values of the control group by 1.61 times, whereas under combined treatment this effect was detected as early as 1 h after exposure (1.32 times relative to the control group). Analysis of ion homeostasis revealed that riboflavin treatment, particularly in combination with laser irradiation, led to an increase in intracellular $Ca^{2+}$ levels (up to 1.9-fold relative to the control at 6 h after exposure). This was accompanied by an increase in $Na^+$ levels and a decrease in $K^+$ levels, with minimal $K^+$ values observed at 6 h after exposure (approximately 0.6 of the control level). Overall, the results demonstrate the photosensitizing activity of riboflavin and support its further investigation in photodynamic approaches for melanoma. The observed effects provide a basis for further investigation of riboflavin-mediated PDT in combination with other anticancer agents to enhance therapeutic efficacy.

**Keywords:** photodynamic therapy; riboflavin; B16-F10 melanoma; blue laser light; apoptosis; ion homeostasis.

Paper #9451 received 11 Dec 2025; revised manuscript received 03 Apr 2026; accepted for publication 01 May 2026; published online 30 Jun 2026. doi: 10.18287/JBPE26.12.020312.

## 1 Introduction

Modern treatment methods of malignant tumors, including surgery, chemotherapy, and radiotherapy, are often associated with pronounced side effects and the development of drug resistance. In recent years, more attention has been paid to minimally invasive and targeted approaches aimed at selectively destroying tumor cells with minimal damage to surrounding tissues [1, 2]. In this context, photodynamic therapy is considered as an alternative approach that minimizes systemic exposure and increases selectivity for tumor cells [3].

Photodynamic therapy (PDT) continues to attract attention as a safe and locally targeted antitumor therapy method that combines the use of a photosensitizer, light of a specific wavelength, and oxygen to generate reactive oxygen species (ROS). The efficacy of PDT is largely

determined by the properties of the photosensitizer: its ability to accumulate in tumor cells selectively, photostability, and minimal toxicity to normal tissues.

Among natural photosensitizers, riboflavin (vitamin $B_2$) and its derivatives stand out due to their high biocompatibility and endogeneity. Riboflavin is a precursor of the coenzymes flavin mononucleotide (FMN) and flavin adenine dinucleotide (FAD), which are involved in mitochondrial redox processes, reducing the risk of long-term toxicity [4]. FMN often functions as a cofactor in membrane-bound flavoproteins (i.e., it is embedded in a protein complex), and such complexes are localized near membranes and enzymatic electron transfer centers [5]. The localization of flavin cofactors near membrane proteins creates a "spot" formation of ROS near the lipid layer, which increases the probability of damage to membrane components during photosensitization [6]. Under the influence of blue light, flavins effectively generate ROS, including singlet oxygen and superoxide, causing damage to cellular structures and inducing a phototoxic effect [7].

Cutaneous melanoma, one of the most aggressive forms of tumors, exhibits high metastatic activity and resistance to systemic therapies which makes localized therapies particularly important [8]. Riboflavin-based photodynamic therapy (PDT) for melanoma seems to be a promising treatment method: low systemic toxicity, selective tumor targeting, and potential for combination with other therapeutic approaches provide the basis for treatment optimization [9].

Despite progress in studying the photodynamic properties of riboflavin, the effect of photosensitizer concentration on the efficacy of PDT for melanoma remains understudied. There is also limited data on how photodynamic action of riboflavin influences intracellular ion homeostasis – the concentrations of $Ca^{2+}$, $K^+$, and $Na^+$, which play a key role in regulating apoptosis and necrosis. Understanding these relationships will not only help to clarify the mechanisms of phototoxicity but also optimize PDT parameters to increase its selectivity and therapeutic potential. Therefore, this study aims to evaluate the relationship between the photodynamic efficacy of riboflavin and its concentration and analyze the associated changes in ionic balance in melanoma cells. Unlike most studies focused primarily on the general phototoxicity of riboflavin, the present work provides a time-resolved analysis of the relationship between apoptosis- and PI-associated signals and changes in $Na^+$-, $K^+$-, and $Ca^{2+}$-associated fluorescence in B16-F10 melanoma cells following photoactivation of riboflavin with blue light. In addition, intracellular ROS generation was assessed to further support the photodynamic mechanism of action.

## 2 Methods and Materials

B16-F10 murine melanoma cell culture was used in the experiments. Cells were obtained from the American Type Culture Collection (ATCC).

The experimental scheme is illustrated in Fig. 1.

Murine melanoma B16-F10 cells were cultured in a Sanyo MCO-18AIC incubator (Helicon, Japan) at 37 °C in a humidified atmosphere containing 5% $CO_2$. Cells were maintained in RPMI-1640 medium (PanEco, Russia) supplemented with 10% fetal bovine serum (Biosera, France) and 80 mg/L gentamicin (PanEco, Russia). One day prior to the experiment, cells were seeded into 8-well chamber slides (SPL Lifesciences, South Korea) at a density of $5 \times 10^4$ cells per well.

### *2.1 Experimental Design*

The following experimental groups were established:

- Control – cells without riboflavin and without laser irradiation;
- IR – cells exposed to laser irradiation only;
- RBF – cells treated with riboflavin only;
- IR + RBF – cells treated with riboflavin followed by laser irradiation.

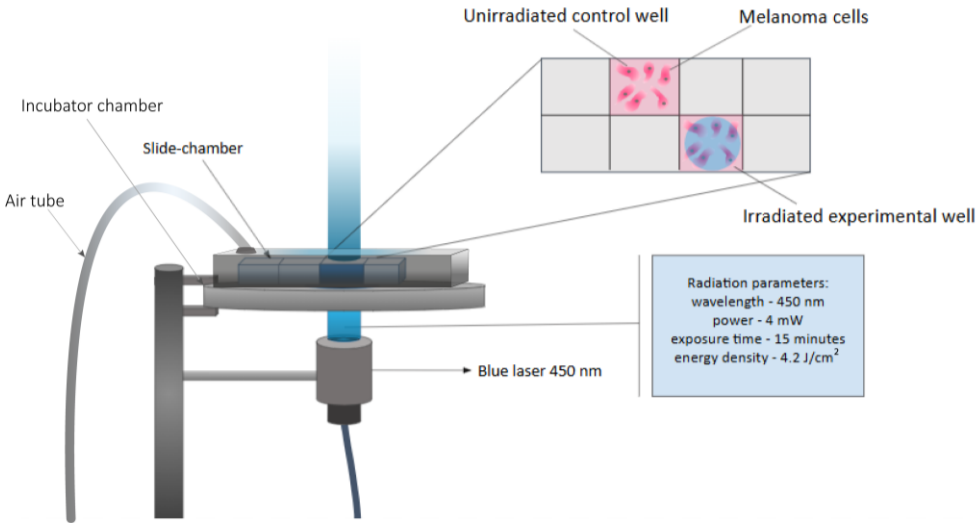


Fig. 1 Experimental scheme.

## 2.2 Laser Irradiation

Irradiation was carried out in a UNO H501-T benchtop incubator (Okolab, Italy) under standard culture conditions. Cells were irradiated using a 450 nm laser diode (MDL-111-450, Changchun New Industries Optoelectronics Tech, China) with an output power of 4 mW. The irradiation time was 15 min, corresponding to an energy density of 4.2 J/cm$^2$ over an exposed area of 0.857 cm$^2$.

The energy density ($E$, J/cm$^2$) was calculated as:

$$E = (P \times t) / S,$$

where $P$ is the output power (W), $t$ is the irradiation time (s), and $S$ is the exposed area (cm$^2$).

## 2.3 Fluorescence Microscopy and Image Analysis

Fluorescence images were acquired using a Nikon Ti-S (Nikon Corporation, Tokyo, Japan) inverted microscope. Image analysis was performed using ImageJ software (NIH, USA).

Quantitative analysis was based on the corrected total cell fluorescence (CTCF) parameter.

For each experimental group, three fields of view were analyzed per experiment. For each field, paired images were acquired: a brightfield image to define cell boundaries and the corresponding fluorescence image.

Brightfield and fluorescence images were overlaid to ensure accurate alignment of cell contours with fluorescence signals. Cell boundaries were manually delineated as regions of interest (ROI) based on visible cell contours. A total of 50 cells were analyzed per field of view, resulting in 150 analyzed cells per group.

For each ROI, the following parameters were measured: area and integrated density.

Background fluorescence was determined individually for each field of view by selecting five regions devoid of cells and calculating the mean background intensity.

CTCF was calculated using the following Eq.:

$$CTCF = ID - (A \times B),$$

where $CTCF$ is the corrected total cell fluorescence; $ID$ is the integrated density; $A$ is the area of the selected region of interest (ROI); and $B$ is the mean background fluorescence of the corresponding microscopic field. Fluorescence values were normalized to the control group and expressed in relative units.

## 2.4 Selection of Riboflavin Concentration

A preliminary experiment was performed to determine the working concentration of the photosensitizer. Riboflavin in the form of flavin mononucleotide (Pharmstandard -UfaVITA, Russia) was applied at concentrations of 10, 50, and 100 μM. After 24 h of culture, the medium was replaced with fresh medium containing riboflavin, and cells were incubated for 90 min in the dark. Subsequently, cells were washed with phosphate-buffered saline (PBS, pH 7.4). These measurements correspond to a preliminary concentration-dependent experiment (3 h time point).

Cell death was assessed 3 h after treatment using Yo-PRO-1 and propidium iodide (PI) at a final concentration of 1 μM each.

## 2.5 Dynamics of Cell Death

Cell death was evaluated using the fluorescent dyes Yo-PRO-1 and propidium iodide (PI) at a final concentration of 1 μM each. Measurements were performed at 1, 6, and 18 h after irradiation. Cells positive for Yo-PRO-1 staining were classified as early apoptotic cells, whereas PI-positive cells were considered to have compromised plasma membrane integrity, corresponding to late apoptosis or necrosis.

## 2.6 Assessment of Intracellular ROS Levels

Intracellular reactive oxygen species (ROS) levels were evaluated using the fluorescent probe 2′,7′-dichlorodihydrofluorescein diacetate (DCFH-DA). Cells were incubated with DCFH-DA at a final concentration of 10 μM for 30 min at 37 °C in the dark. After incubation, cells were washed with phosphate-buffered saline (PBS, pH 7.4) to remove excess probe.

Fluorescence measurements were performed immediately after photodynamic treatment and 3 h later.

Fluorescence images were acquired using a Nikon Ti-S (Nikon Corporation, Tokyo, Japan) inverted microscope under identical acquisition settings for all experimental groups. Quantitative analysis was performed using ImageJ software (NIH, USA) based on the CTCF parameter, as described below.

## 2.7 MTT Assay

After irradiation, the medium was removed and replaced with an equal volume of fresh pre-warmed culture medium. Cells were incubated for 3 h in a humidified $CO_2$ incubator at 37 °C. After this incubation period, the medium was removed and replaced with 100 μL of fresh warm medium containing 10 μL of MTT solution (5 mg/mL; PanEco, Russia). Cells were additionally incubated for 3 h at 37 °C in a $CO_2$ incubator.

After incubation, 100 μL of solubilization solution was added to each well to dissolve intracellular formazan crystals. The solubilization solution consisted of 99.4 mL dimethyl sulfoxide (Helicon, Russian Federation), 0.6 mL glacial acetic acid (Ecos-1, Russia), and 10 g sodium dodecyl sulfate (PanEco, Russian Federation). The contents of the wells were then aspirated and transferred to a 96-well plate. Absorbance was measured using a Multiskan FC plate reader (Thermo Scientific, USA) at 620 nm. Cell viability in each well was calculated relative to the absorbance value of the control group, followed by graphical presentation of the data.

### *2.8 LDH Assay*

After irradiation, the medium was removed and replaced with an equal volume of fresh pre-warmed culture medium. Cells were incubated for 3 h in a humidified $CO_2$ incubator at 37 °C. After incubation, the culture medium from each well was collected into precooled microcentrifuge tubes and centrifuged for 10 min at 1500 × g. The supernatant was transferred into fresh precooled tubes.

After medium removal, 500 µL of cold PBS was added to each well, collected into microcentrifuge tubes, and centrifuged for 5 min at 1500 rpm. The supernatant was discarded. Then, 100 µL of lysis buffer (Cloud-Clone Corp., China) was added to each well, and the plate was additionally incubated for 30 min at room temperature. The lysates were collected into tubes containing the cell pellet and centrifuged for 30 min at 1500 × g. Then, 90 µL of the resulting supernatant was diluted in 360 µL of cold PBS.

LDH concentration was measured using an ERBA XL-100 biochemical analyzer (Erba Lachema, Czech Republic) with a Lactate Dehydrogenase-P kit (Erba Lachema, Czech Republic). The data were calculated as the concentration of LDH released into the medium relative to the LDH concentration in the corresponding cell lysate.

### *2.9 Intracellular Ion Levels*

Intracellular ion levels were evaluated using the fluorescent dyes Rhod-2 AM, ION NatriumGreen 2 AM, and ION PotassiumGreen 2 AM at a final concentration of 1 µM each. Measurements were performed at 1, 6, and 18 h after irradiation. Fluorescence intensity of ion-sensitive dyes was interpreted as a relative indicator of changes in intracellular $Ca^{2+}$, $Na^{+}$, and $K^{+}$ levels rather than a direct quantitative measurement of absolute ion concentrations.

### *2.10 Statistical Analysis*

All experiments were performed in at least three independent replicates. Statistical analysis was carried out using Microsoft Excel. Differences between groups were evaluated using the Mann–Whitney *U*-test. Results were considered statistically significant at $p \leq 0.05$.

## 3 Results

### *3.1 Selection of Riboflavin Concentration*

Incubation of B16-F10 murine melanoma cells with the photosensitizer riboflavin showed a direct relationship between riboflavin concentration and the level of apoptosis (Fig. 2(a)).

As follows from Fig. 2(a), there is a noticeable The data presented in Fig. 2(b) show that B16-F10 cells treated with riboflavin at concentrations of 10, 50, and 100 µM and exposed to laser irradiation exhibited an increased level of apoptotic cells, with the maximum observed at a concentration of 50 µM (2.2-fold higher than in the control group).

Figure 3 presents the results of the study examining the effects of riboflavin and laser irradiation on necrotic cell death in B16-F10 melanoma cells.

A comparative analysis showed that the level of necrosis in cells treated with riboflavin at a concentration of 10 µM and exposed to laser irradiation was significantly lower than in the corresponding non-irradiated group. The CTCF values for incubation with riboflavin at concentrations of 50 and 100 µM in the study groups did not differ significantly.

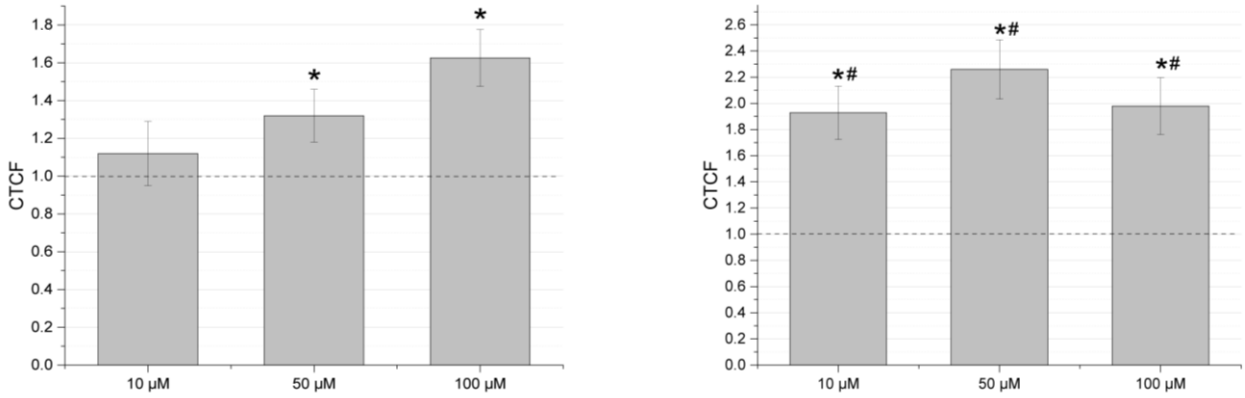


(a) (b)

Fig. 2 (a) Effect of riboflavin concentration on apoptosis in B16-F10 melanoma cells. (b) Effect of riboflavin concentration combined with laser irradiation (450 nm, 4.2 J/cm²) on apoptosis in B16-F10 melanoma cells 3 h after exposure. Fluorescence intensity is presented as corrected total cell fluorescence (CTCF) normalized to the control group. * $p < 0.05$ vs control; # $p < 0.05$ vs irradiated group.

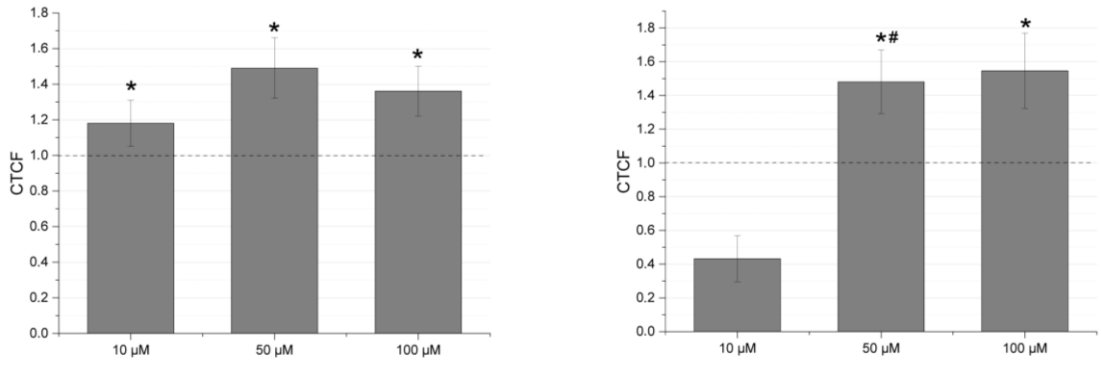


(a) (b)

Fig. 3 (a) Effect of riboflavin concentration on necrosis in B16-F10 melanoma cells. (b) Effect of riboflavin concentration combined with laser irradiation (450 nm, 4.2 J/cm²) on necrosis in B16-F10 melanoma cells 3 h after exposure. Fluorescence intensity is presented as corrected total cell fluorescence (CTCF) normalized to the control group. * $p < 0.05$ vs control; # $p < 0.05$ vs irradiated group.

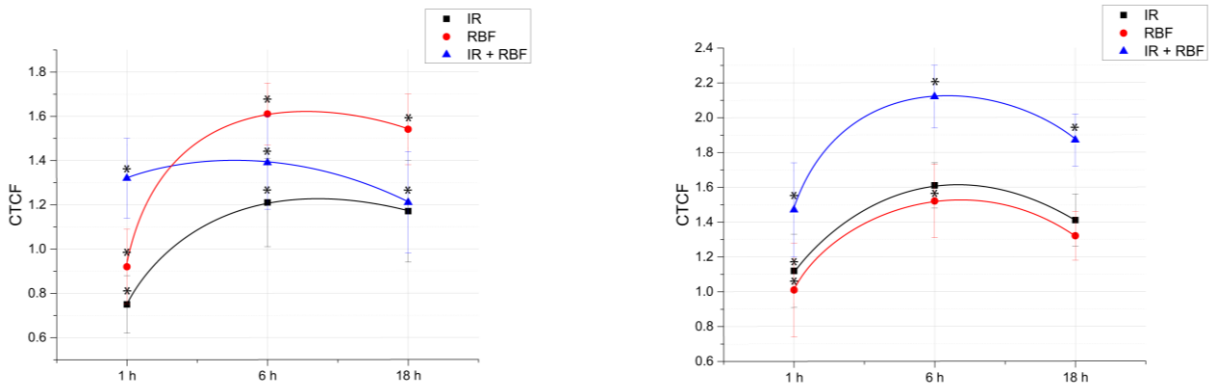


(a) (b)

Fig. 4 Dynamics of cell death in B16-F10 melanoma cells at 1, 6, and 18 h after treatment. (a) Apoptosis. (b) Necrosis. Fluorescence intensity is presented as corrected total cell fluorescence (CTCF) normalized to the control group. IR – laser irradiation (450 nm, 4.2 J/cm²); RBF – riboflavin (50 μM); IR+RBF – combined treatment with riboflavin and laser irradiation. * $p < 0.05$ compared with the control group.

### *3.2 Dynamics of Cell Death*

Figure 4 shows the dynamics of cell death in B16-F10 melanoma cells.

In all experimental groups, an increase in cell death was observed 6 h after treatment, followed by a decrease by 18 h.

Analysis of apoptotic cell death in melanoma cells showed that the highest levels were observed in the combined treatment group, reaching a maximum of 2.12-fold at 6 h after treatment. In the single-treatment groups, CTCF values varied only slightly throughout the observation period.

Analysis of necrotic cell death showed that the highest level was observed in the riboflavin group, reaching the value of 1.61 higher relative to the control group at 6 h. Laser irradiation alone did not result in significant changes. In contrast, combined treatment induced earlier necrotic cell death: at 1 h after treatment, CTCF levels were 1.32 times higher than in the control group, while remaining lower in the other experimental groups.

These results indicate that the combined treatment with riboflavin and laser irradiation enhances cell death and accelerates the onset of necrotic processes.

### *3.3 Intracellular ROS Generation*

As shown in Fig. 5, the results showed that immediately after exposure, the level of reactive oxygen species in the laser irradiation group was 1.46 relative to the control, while in the riboflavin group it was 1.20. The combined exposure to laser irradiation and riboflavin led to the most pronounced increase in reactive oxygen species levels, reaching 1.84 relative to the control.

At 3 h after exposure, an increase in reactive oxygen species levels was also observed under combined exposure, reaching 1.39 relative to the control. The combined exposure to laser irradiation and riboflavin was observed to enhance the generation of reactive oxygen species, which is consistent with a photodynamic mechanism of action.

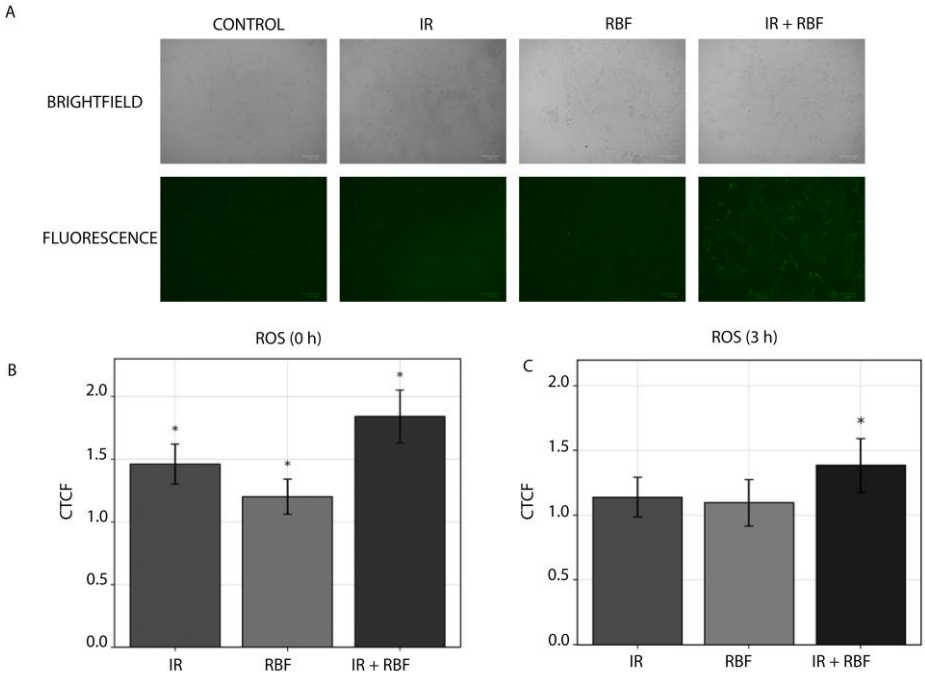


Fig. 5 Intracellular reactive oxygen species (ROS) levels in B16-F10 melanoma cells after photodynamic treatment. (A) Representative brightfield and fluorescence images of B16-F10 melanoma cells. The upper row shows brightfield images, and the lower row shows fluorescence corresponding to intracellular ROS detected using the DCFH-DA probe. Images were obtained immediately after treatment. (B) Intracellular ROS levels immediately after treatment. (C) Intracellular ROS levels 3 h after treatment. Fluorescence intensity is presented as corrected total cell fluorescence (CTCF) normalized to the control group. Data are presented as mean ± SD. Experimental groups: Control – untreated cells; IR – laser irradiation (450 nm, 4.2 J/cm²); RBF – riboflavin (50 μM); IR+RBF — combined treatment with riboflavin and laser irradiation. * $p < 0.05$ compared with the control group.

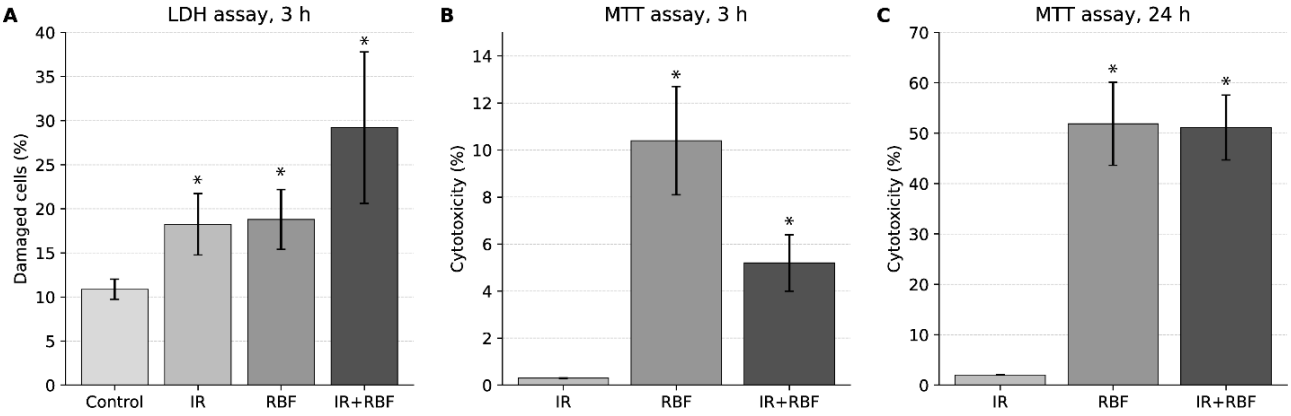


Fig. 6 Assessment of membrane damage and metabolic activity in B16-F10 melanoma cells after photodynamic treatment. (A) LDH assay, 3 h, (B) MTT assay, 3 h, (C) MTT assay, 24 h. The LDH assay reflects membrane integrity, whereas the MTT assay evaluates cellular metabolic activity. Data are presented as mean ± SD. IR – laser irradiation (450 nm, 4.2 J/cm²); RBF – riboflavin (50 μM); IR+RBF – combined treatment with riboflavin and laser irradiation. * $p < 0.05$ compared with the control group.

### *3.4 Membrane Damage and Metabolic Activity*

The effects of photodynamic treatment on membrane integrity and metabolic activity of B16-F10 melanoma cells were assessed using LDH and MTT assays (Fig. 6).

At 3 h after treatment, the LDH assay demonstrated an increased proportion of damaged cells in all experimental groups compared with the control group. The highest level of membrane damage was observed in the group with combined exposure to laser irradiation and riboflavin (29.21%), while the laser irradiation group and the riboflavin group showed comparable values (18.25% and 18.79%, respectively) relative to the control group (10.87%).

According to the MTT assay, decrease in metabolic activity at 3 h remained low in all groups, reaching 0.3% in the laser irradiation group, 10.4% in the riboflavin group, and 5.2% in the group with combined exposure.

At 24 h, a pronounced decrease in metabolic activity was observed in the riboflavin group (51.87%) and in the group with combined exposure (51.15%), whereas the laser irradiation group showed only minimal changes (2.01%).

### *3.5 Changes in Intracellular Sodium Levels*

Figure 7 shows the dynamics of changes in intracellular sodium levels in B16-F10 melanoma cells. High sodium levels were observed in the experimental groups 6 h after exposure (up to ~2.6 times in the RBF group and ~2.0 times in the IR+RBF group relative to the control group). However, the values in the group exposed only to riboflavin were significantly higher than in both the combined treatment group and the laser irradiation group. After 18 h, a decrease in sodium levels was observed in all study groups, approaching ~1.1–1.3-times relative to the control group.

### *3.6 Changes in Intracellular Calcium Levels*

Changes in intracellular calcium levels are presented in Fig. 8. Figure 8 shows changes in intracellular calcium levels in the B16-F10 cell culture at 1, 6, and 18 h after exposure. Exposure to the photosensitizer, both alone and in combination with laser irradiation, results in a marked increase in calcium levels, reaching ~1.6 times higher at 1 h and peaking at ~1.9–2.0 at 6 h relative to the control group. Calcium levels then remain elevated but begin to decline by 18 h (~1.4–1.6-fold). In the group exposed only to laser irradiation, minimal changes in calcium levels were observed at all-time intervals studied (~0.8–0.9 times relative to the control group).

### *3.7 Changes in Intracellular Potassium Levels*

As shown in Fig. 9, a significant decrease in potassium levels was observed 6 h after exposure in all study groups (to ~0.7–0.8 times higher relative to the control group). In the groups exposed to laser irradiation or riboflavin, a further decrease in potassium levels was observed after 18 h (to ~0.6–1.1-fold). In contrast, in the group that received the combined treatment, potassium levels increased by 18 h (~1.2–1.3-fold) and remained the highest among all study groups.

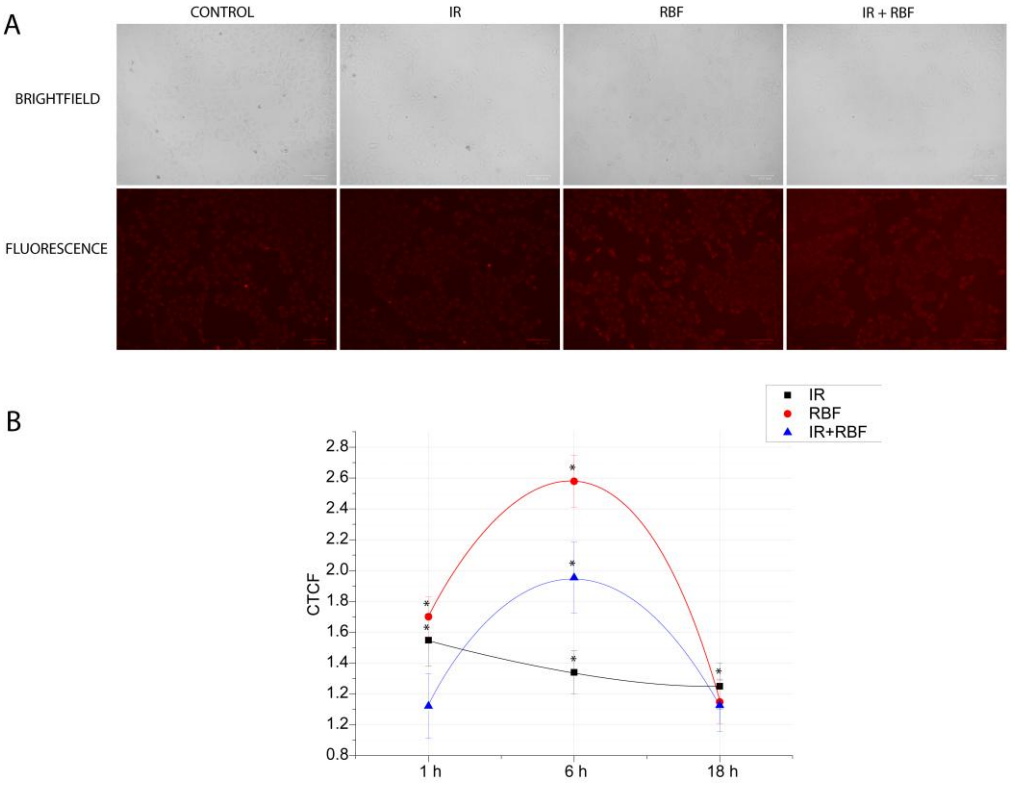


Fig. 7 Intracellular sodium dynamics in B16-F10 melanoma cells after photodynamic treatment. (A) Representative brightfield and fluorescence images of B16-F10 cells in the Control, IR, RBF, and IR+RBF groups. The upper row shows brightfield images, and the lower row shows fluorescence corresponding to intracellular sodium levels. Images were obtained 1 h after treatment. (B) Time-dependent changes in intracellular sodium levels at 1, 6, and 18 h after treatment. Fluorescence intensity is presented as corrected total cell fluorescence (CTCF) normalized to the control group. Data are presented as mean ± SD. IR – laser irradiation (450 nm, 4.2 J/cm$^2$); RBF – riboflavin (50 μM); IR+RBF – combined treatment with riboflavin and laser irradiation. * $p < 0.05$ compared with the control group.

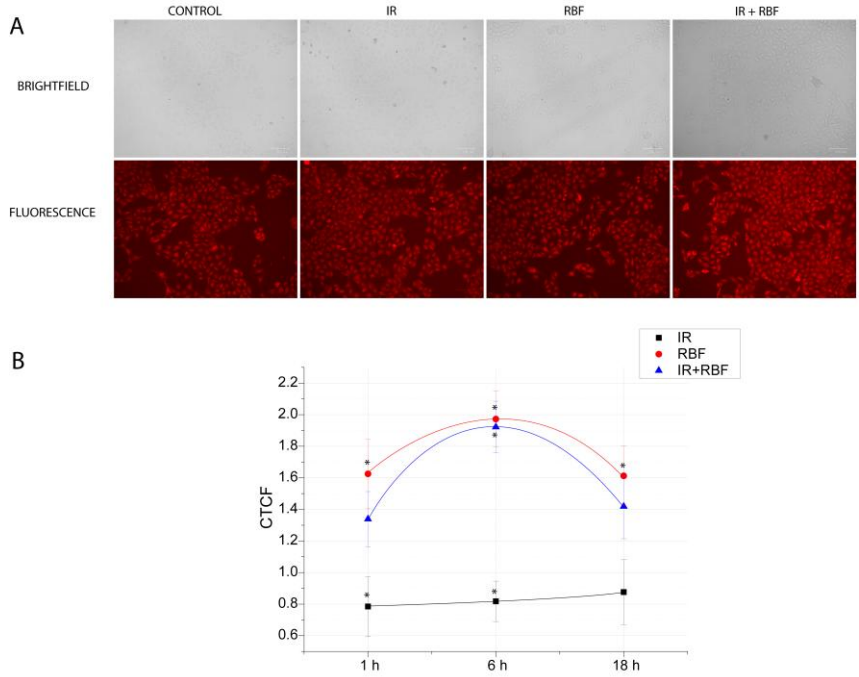


Fig. 8 Intracellular calcium dynamics in B16-F10 melanoma cells after photodynamic treatment. (A) Representative brightfield and fluorescence images of B16-F10 cells in the Control, IR, RBF, and IR+RBF groups. The upper row shows brightfield images, and the lower row shows fluorescence corresponding to intracellular calcium levels. Images were obtained 1 h after treatment. (B) Time-dependent changes in intracellular calcium levels at 1, 6, and 18 h after treatment. Fluorescence intensity is presented as corrected total cell fluorescence (CTCF) normalized to the control group. Data are presented as mean ± SD. IR – laser irradiation (450 nm, 4.2 J/cm$^2$); RBF – riboflavin (50 μM); IR+RBF – combined treatment with riboflavin and laser irradiation. * $p < 0.05$ compared with the control group.

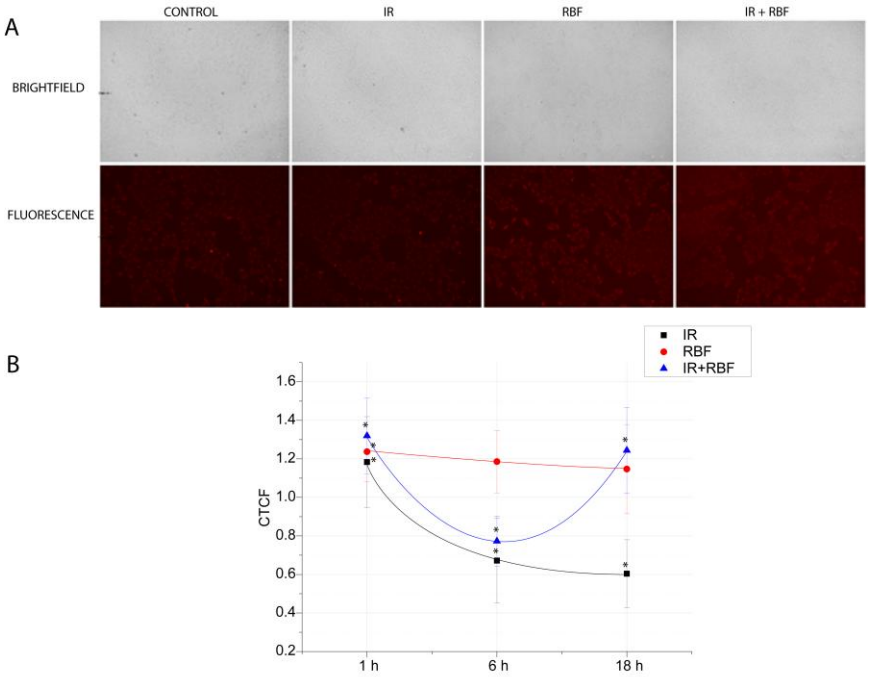


Fig. 9 Intracellular potassium dynamics in B16-F10 melanoma cells after photodynamic treatment. (A) Representative brightfield and fluorescence images of B16-F10 cells in the Control, IR, RBF, and IR+RBF groups. The upper row shows brightfield images, and the lower row shows fluorescence corresponding to intracellular potassium levels. Images were obtained 1 h after treatment. (B) Time-dependent changes in intracellular potassium levels at 1, 6, and 18 h after treatment. Fluorescence intensity is presented as corrected total cell fluorescence (CTCF) normalized to the control group. Data are presented as mean ± SD. IR – laser irradiation (450 nm, 4.2 J/cm$^2$); RBF – riboflavin (50 μM); IR+RBF – combined treatment with riboflavin and laser irradiation. *$p < 0.05$ compared with the control group.

## 4 Discussion

In this study, using the B16-F10 cell line model, we demonstrated the significant cytotoxic activity of riboflavin in combination with blue laser irradiation ($\lambda$ = 450 nm, $E$ = 4.2 J/cm²) and identified key features associated with changes in ion homeostasis and the temporal dynamics of apoptosis/necrosis.

In the vast majority of studies, free riboflavin (and related water-soluble flavins FMN, FAD, and derivatives) exhibit little or no cytotoxicity in the dark at typical concentrations used for photo-dynamics – most cell death occurs upon photo-activation [10, 11]. Our results demonstrate that riboflavin induces apoptosis and necrosis in B16-F10 cells in the absence of laser photo-activation, indicating its dark toxicity starting at a concentration of 10 μM. These data are inconsistent with the results previously published by Insińska-Rak et al., who found no cytotoxicity at concentrations up to 50 μM [12], as well as with data by Akasov et al., who reported the safety of riboflavin up to 100 μM [13], and other studies [14]. This may be associated with the participation of riboflavin in metabolic processes and the ability to oxidize and reduce partially the effect on intracellular structures.

The effectiveness of a photosensitizer in PDT directly depends on its concentration. At moderate doses, ROS generation occurs at levels sufficient to trigger caspase-dependent apoptosis, but insufficient to cause uncontrolled damage to cell membranes and organelles. At high concentrations, excessive ROS generation is observed, leading to photo-destruction, decreased selectivity, and a switch to a necrotic cell death pathway [15]. In our experiments, photo-activation with blue laser radiation significantly enhanced apoptotic processes, with the maximum effect achieved at 50 μM riboflavin, after which a decrease in apoptosis and necrosis became predominant at 100 μM. These data are consistent with the results on the effect of flavin mononucleotide in melanoma cell lines, where $IC_{50}$ were in the range of ~10–30 μM under 450 nm irradiation [13], and the peak of necrosis was noted at 100 μM. Thus, a concentration of 50 μM can be considered optimal, since at this concentration apoptosis dominates over necrosis, which is preferable from a therapeutic point of view [16].

The temporal dynamics of cell death (at 50 μM riboflavin) reveals additional details. The peak of cell death for all groups is observed approximately 6 h after treatment, especially apoptosis with combined exposure, which correlates with the mechanisms of photodynamic therapy, in which ROS generation and organelle damage trigger caspase-dependent pathways within the first few hours after irradiation [17]. The early phase of necrosis observed in our data indicates rapid oxidative damage to membranes, which leads to a necrotic outcome even before apoptosis. A higher proportion of necrotic cells in the group treated with riboflavin without irradiation indicates the predominance of disordered forms of cell death, most likely associated with redox stress and direct membrane damage. With photodynamic exposure, a redistribution towards apoptosis is observed, which is consistent with a caspase-dependent mechanism and singlet oxygen generation. One can assume that photo-activation of riboflavin not only enhances its cytotoxicity but also shifts the cellular response from a necrotic to an apoptotic state. The decrease in the apoptotic fraction by 18 h probably reflects either the further transformation of apoptosis into late necrosis or the removal of apoptotic bodies from the culture and the inability to detect them with a fluorescent dye [18].

Our data show that melanoma cells treated with riboflavin, laser irradiation, and their combination undergo significant changes in ion concentration, suggesting profound ion dysregulation as part of the cellular response. This dysregulation includes $Na^+$ influx, $K^+$ efflux or reorganization, and $Ca^{2+}$ overload or reduction, depending on the type of treatment and time point. The observed maximum change in the concentration of most ions at ~6 h after treatment is consistent with the temporal concept of the photodynamic response: the initial phase (1 h) is characterized by early disruption of membrane barrier function; by 6 h, ROS-mediated damage to organelles and channels accumulates and apoptotic mechanisms are triggered; and by 18 h, either compensatory mechanisms are activated or cell death occurs.

A significant increase in intracellular $Na^+$ is observed with both non-irradiated and irradiated riboflavin treatment, particularly pronounced by 6 h. This effect may be caused by ROS-mediated membrane damage and decreased $Na^+/K^+$ ATPase activity, which increases $Na^+$ permeability, disrupts ionic balance, and promotes cell stress and death. This mechanism is supported by experimental data, where an increase in $Na^+$ inside tumor cells led to their death [19].

One hour after treatment with riboflavin and the combined exposure, a moderate increase in intracellular $K^+$ is observed, reflecting the early adaptive activity of $K^+$ channels and an attempt to maintain homeostasis. At the point of 6 h, coinciding with the peak of apoptosis and necrosis, a sharp decrease in $K^+$ and a simultaneous increase in $Na^+$ are observed. A drop in $K^+$ facilitates the activation of caspases and the implementation of apoptosis, and an increase in $Na^+$ reflects a disruption in membrane permeability and a compensatory response to osmotic imbalance, which may also indicate partial necrotic cell damage [20, 21].

With riboflavin, and especially with combined exposure, a significant increase in intracellular $Ca^{2+}$ (up to 1.9 by 6 h) was also observed. ROS-mediated damage to the endoplasmic reticulum and mitochondria can cause the release of $Ca^{2+}$ from internal stores or enhance its entry from the outside through channels, consistent with the dynamics of $K^+$ and $Na^+$. This is confirmed by reviews on melanoma, where calcium signaling plays a key role in apoptosis and the vulnerability of melanoma cells, as well as in the control of the stress response and drug sensitivity [22]. With exposure of laser alone, $Ca^{2+}$ decreased (up to 0.8 times), which may indicate the activation of compensatory mechanisms, such as increased extrusion of $Ca^{2+}$ or limitation of release from

stores. Modern approaches to photodynamic therapy for melanoma confirm a direct link between ROS generation, $Ca^{2+}$ changes and cell death [23, 24].

By 18 h of combined exposure, $K^+$ levels are restored above baseline values, and $Na^+$ levels stabilize, indicating the survival of some cells and restoration of ionic balance. In general, the dynamics of $Na^+$, $K^+$, and $Ca^{2+}$ may reflect the following sequence: early adaptation → apoptotic/necrotic phase with a decrease in $K^+$ and an increase in $Na^+$, and an increase in $Ca^{2+}$ → recovery of some cells and restoration of ionic homeostasis.

The obtained results on intracellular ROS levels, as well as MTT and LDH assays, further support the proposed mechanisms of photodynamic action. The pronounced increase in ROS generation observed immediately after combined treatment confirms the key role of oxidative stress in initiating cell death. The LDH assay demonstrated early membrane damage at 3 h, particularly in the combined treatment group, indicating disruption of membrane integrity under photodynamic conditions. At the same time, the MTT assay showed a delayed decrease in metabolic activity, with a marked increase in cytotoxicity at 24 h, especially in the riboflavin and combined treatment groups. This suggests that metabolic impairment develops progressively following the initial oxidative and membrane damage. Together, these findings indicate that photodynamic exposure induces a cascade of events including ROS generation, membrane disruption, and subsequent loss of cellular metabolic activity.

## 5 Conclusion

This study demonstrates that riboflavin exhibits photosensitizing activity in B16-F10 melanoma cells and enhances cytotoxic effects upon blue laser irradiation. In addition, measurable cytotoxicity was observed in the absence of irradiation, which should be interpreted with caution and may depend on specific experimental conditions.

The combined use of riboflavin and laser irradiation was associated with increased ROS generation and disruption of ion homeostasis, including alterations in $Na^+$, $K^+$, and $Ca^{2+}$ levels, which is consistent with enhanced cell death.

These findings suggest that riboflavin-mediated photodynamic treatment may contribute to cytotoxic effects in melanoma cells and provide a basis for further investigation of its potential application in combination with other therapeutic strategies.

## Acknowledgments

This work was done under the financial support of the Ministry of Science and Higher Education of the Russian Federation (Project No. FEUF-2025-0001 (125041105147-5)).

## Disclosures

All authors declare that there is no conflict of interest in this paper.

## References

1. R. Kaur, A. Bhardwaj, and S. Gupta, "Cancer treatment therapies: traditional to modern approaches to combat cancers," Molecular Biology Reports 50(11), 9663–9676 (2023).
2. D. T. Michaeli, J. C. Michaeli, and T. Michaeli, "Advances in cancer therapy: clinical benefit of new cancer drugs," Aging 15(12), 5232–5234 (2023).
3. Y. Allamyradov, J. Ben Yosef, B. Annamuradov, M. Ateyeh, C. Street, H. Whipple, and A. O. Er, "Photodynamic therapy review: past, present, future, opportunities and challenges," Photochem 4(4), 434–461 (2024).
4. M. Insińska-Rak, M. Sikorski, and A. Wolnicka-Glubisz, "Riboflavin and its derivates as potential photosensitizers in the photodynamic treatment of skin cancers," Cells 12(18), 2304 (2023).
5. P. Carpentier, F. Pierrel, N. Duraffourg, B. Guigliarelli, M. Hajj Chehade, L. Flandrin, C. Basset, C. Caux, S. Torelli, and V. Nivière, "Studies of the membrane-bound flavocytochrome MsrQ flavin mononucleotide ( FMN )-binding site reveal an unexpected ubiquinone cofactor," The FEBS Journal 292(20), 5491–5505 (2025).
6. A. Okamoto, S. Kalathil, X. Deng, K. Hashimoto, R. Nakamura, and K. H. Nealson, "Cell-secreted flavins bound to membrane cytochromes dictate electron transfer reactions to surfaces with diverse charge and pH," Scientific Reports 4(1), 5628 (2014).
7. M. Insińska-Rak, M. Sikorski, "Riboflavin interactions with oxygen-a survey from the photochemical perspective," Chemistry – A European Journal 20(47), 15280–15291 (2014).
8. M. Hsieh, S.-K. Hsu, T.-Y. Liu, C.-Y. Wu, and C.-C. Chiu, "Melanoma biology and treatment: a review of novel regulated cell death-based approaches," Cancer Cell International 24(1), 63 (2024).
9. G. Gunaydin, M. E. Gedik, and S. Ayan, "Photodynamic therapy—current limitations and novel approaches," Frontiers in Chemistry 9, 691697 (2021).
10. M.-Y. Yang, C.-J. Chang, and L.-Y. Chen, "Blue light induced reactive oxygen species from flavin mononucleotide and flavin adenine dinucleotide on lethality of HeLa cells," Journal of Photochemistry and Photobiology B: Biology 173, 325–332 (2017).
11. A. V. Juarez, L. D. V. Sosa, A. L. De Paul, A. P. Costa, M. Farina, R. B. Leal, A. I. Torres, and P. Pons, "Riboflavin acetate induces apoptosis in squamous carcinoma cells after photodynamic therapy," Journal of Photochemistry and Photobiology B: Biology 153, 445–454 (2015).

12. A. Wolnicka-Glubisz, A. Pawlak, M. Insinska-Rak, and A. Zadlo, "Analysis of photoreactivity and phototoxicity of riboflavin's analogue 3MeTARF," Journal of Photochemistry and Photobiology B: Biology 205, 111820 (2020).
13. R. A. Akasov, N. V. Sholina, D. A. Khochenkov, A. V. Alova, P. V. Gorelkin, A. S. Erofeev, A. N. Generalova, and E. V. Khaydukov, "Photodynamic therapy of melanoma by blue-light photoactivation of flavin mononucleotide," Scientific Reports 9(1), 9679 (2019).
14. S. Kacar, C. Hacioglu, and F. Kar, "Irradiated riboflavin over nonradiated one: Potent antimigratory, antiproliferative and cytotoxic effects on glioblastoma cells," Journal of Cellular and Molecular Medicine 28(8), e18288 (2024).
15. D. L. Sai, J. Lee, D. L. Nguyen, and Y.-P. Kim, "Tailoring photosensitive ROS for advanced photodynamic therapy," Experimental & Molecular Medicine 53(4), 495–504 (2021).
16. D. Machado, S. M. Shishido, K. C. S. Queiroz, D. N. Oliveira, A. L. C. Faria, R. R. Catharino, C. A. Spek, and C. V. Ferreira, "Irradiated riboflavin diminishes the aggressiveness of melanoma *in vitro* and *in vivo*," PLoS ONE 8(1), e54269 (2013).
17. P. Agostinis, K. Berg, K. A. Cengel, T. H. Foster, A. W. Girotti, S. O. Gollnick, S. M. Hahn, M. R. Hamblin, A. Juzeniene, D. Kessel, M. Korbelik, J. Moan, P. Mroz, D. Nowis, J. Piette, B. C. Wilson, and J. Golab, "Photodynamic therapy of cancer: An update," CA: A Cancer Journal for Clinicians 61(4), 250–281 (2011).
18. C. Saenz, M. Ethirajan, E. C. Tracy, M.-J. Bowman, J. Cacaccio, T. Ohulchanskyy, H. Baumann, and R. K. Pandey, "Charged groups on pyropheophorbide-based photosensitizers dictate uptake by tumor cells and photodynamic therapy efficacy," Journal of Photochemistry and Photobiology B: Biology 227, 112375 (2022).
19. N. Clemente, S. Baroni, S. Fiorilla, F. Tasso, S. Reano, C. Borsotti, M. R. Ruggiero, E. Alchera, M. Corrazzari, G. Walker, A. Follenzi, S. G. Crich, and R. Carini, "Boosting intracellular sodium selectively kills hepatocarcinoma cells and induces hepatocellular carcinoma tumor shrinkage in mice," Communications Biology 6, 574 (2023).
20. F. Lang, E. K. Hoffmann, "Role of ion transport in control of apoptotic cell death," Comprehensive Physiology 2(3), 2037–2061 (2012).
21. C. D. Bortner, J. A. Cidlowski, "Cell shrinkage and monovalent cation fluxes: Role in apoptosis," Archives of Biochemistry and Biophysics 462(2), 176–188 (2007).
22. H. Zhang, Z. Chen, A. Zhang, A. A. Gupte, and D. J. Hamilton, "The role of calcium signaling in melanoma," International Journal of Molecular Sciences 23(3), 1010 (2022).
23. W.-H. Chan, "Photodynamic treatment induces an apoptotic pathway involving calcium, nitric oxide, p53, p21-activated kinase 2, and c-Jun N-terminal kinase and inactivates survival signal in human umbilical vein endothelial cells," International Journal of Molecular Sciences 12(2), 1041–1059 (2011).
24. N. Sobhani, A. A. Samadani, "Implications of photodynamic cancer therapy: an overview of PDT mechanisms basically and practically," Journal of the Egyptian National Cancer Institute 33(1), 34 (2021).